Supplementary Materials for

Low Interfacial Toughness (LIT) Materials for Effective Large-Scale De-Icing

Kevin Golovin[1,2†], Abhishek Dhyani[2,3†], M. D. Thouless[1,4*], and Anish Tuteja[1,2,3,5*]

[1]Department of Materials Science and Engineering, [2]Biointerfaces Institute, [3]Macromolecular Science and Engineering, [4]Department of Mechanical Engineering, [5]Department of Chemical Engineering, University of Michigan – Ann Arbor. * indicates corresponding author. † these authors contributed equally.

Corresponding author emails: thouless@umich.edu; atuteja@umich.edu

This PDF file includes:

Supplementary Methods
Supplementary Discussion
Supplementary Figs. S1 to S20
Supplementary Table S1
Captions for Movies S1 to S5

Other Supplementary Materials for this manuscript include the following:

Movies S1 to S5

Compiled data for all figures (.xlsx)

Section 1. Supplementary Methods

A. Synthesis. We evaluated the interfacial properties between ice and many different plastics, purchased from McMaster. These plastics, which all had a thickness of t = 1.58 mm, were ultra-high-molecular-weight polyethylene (UHMWPE; Catalog No. 8752K121), low-density polyethylene (LDPE; Catalog No. 8657K111), polypropylene (PP; Catalog No. 8742K131),

polycarbonate (PC; Catalog No. 8574K24), polystyrene (PS; Catalog No. 8734K32), polymethylmethacrylate (PMMA; Catalog No. 8560K171), glycol-modified polyethylene terephthalate (PETG; Catalog No. 8597K52), nylon (Catalog No. 8539K11), acrylonitrile butadiene styrene (ABS; Catalog No. 8586K152), polyvinylchloride (PVC; Catalog No. 87545K131), chlorinated polyvinylchloride (CPVC; Catalog No. 8748K22), polytetrafluoroethylene (PTFE; Catalog No. 8545K22), and a fiberglass-epoxy laminate (Garolite; Catalog No. 9910T15).

To fabricate coatings of "Silicone B", PDMS (Mold Max™ STROKE from Smooth-On Inc.) was mixed in a 10:1 base:crosslinker ratio, following manufacturer instructions. 2 mL of toluene was added to 10 g of total material, and the mixture was vortexed until homogeneous. For visualization, Oil-Red-O dye (Alfa Aesar) was added to the toluene (10 mg/mL) before mixing with the silicone rubber. The solution was poured onto aluminum (Al) substrates (Al 6061 from McMaster; Catalog No. 89015K143) measuring 6 × 22 × 0.06 cm after sanding (80 Grit and then 1200 Grit) and cleaning. To fabricate "Plasticized Silicone B", a more icephobic coating, the same procedure was followed, but with a mixture of 40 wt% silicone oil (100 cP, Sigma Aldrich) and Silicone B. The two systems were both cured at room temperature overnight. The thicknesses of these coatings were approximately 1 mm.

Another icephobic PDMS, Silicone A, was fabricated from Sylgard 184 (Dow Corning) in a 10:1 base:crosslinker ratio, per manufacturer instructions. The mixture was vortexed until homogeneous, degassed to remove bubbles, and poured onto the same size Al substrates as above. The sample was then cured at 150 °C for 1 hour. To fabricate "Plasticized Silicone A", a more icephobic form, the same procedure was followed, but with a mixture of 25 wt% silicone oil (100 cP, Sigma Aldrich) and Silicone A. As with the previous system, the thickness of these coatings was approximately 1mm.

To fabricate plasticized PVC coatings, polyvinyl chloride (M_w = 120,000, Scientific Polymer) was dissolved in a 60/40 vol% mixture of acetone and *n*-methyl pyrrolidone (NMP, Sigma Aldrich) at four different concentrations, 200 mg/mL, 100 mg/mL, 50 mg/mL, and 25 mg/mL, to generate a range of coating thicknesses. Once fully dissolved, medium-chain triglyceride oil (MCT, Jedwards International) was added to the solution at 0, 5, 10 or 50 wt%, to generate four different levels of plasticization. The systems were homogenized using a vortexer at room temperature. After homogenization, the solutions were poured onto aluminum substrates. The coated Al samples were placed on a 35 °C hotplate for 10 minutes to evaporate the acetone, and then a 70 °C hotplate overnight to remove the NMP. This resulted in coatings with different thicknesses ranging from 1 μm to 150 μm (as measured using a Mitotoyo micrometer), depending on the initial concentration. All the coatings exhibited a similar ratio of advancing contact angle to receding contact angle of θ_{adv} / θ_{rec} = 92° / 80°.

Three specimens were designated as having Low Interfacial Toughness (LIT); these were very thin coatings of the PDMS, PVC and PS. The "LIT PDMS" coating was fabricated by forming a solution of Silicone B and 40 wt% silicone oil in hexane at an overall concentration of 25 mg/mL. This resulted in a coating of about 1 μm. The "LIT PVC" coating was made as described above to form the thinnest coating of about 1 to 2 μm, with 50% MCT, at an overall solution concentration of 25 mg/mL. The "LIT PS" coating was fabricated by forming a solution

of polystyrene (M_w = 40,000, Scientific Polymer) and 20 wt% diisodecyl adipate (DIDA) in toluene at an overall concentration of 25 mg/mL. This also resulted in a coating with a thickness of about 1 μm.

B. Ice adhesion measurement. The measurements of τ_{ice} and $\tilde{F}_{ice}$ were conducted in a similar fashion to techniques reported previously *(2, 25, 26)*. However, two differences are worth noting. First, to observe a critical length during ice-adhesion testing, a larger Peltier-plate system was required. The Peltier-plate system used in this work (Laird Technologies) measured 22 cm in length and 6 cm in width (Fig. 1D). The sample to be tested was prepared to fit this geometry and adhered to the plate using double-sided tape (3M Company). Second, to evaluate different lengths of interfacial area in a relatively short amount of time, and to maximize consistency between tests, the entire substrate was used for ice-adhesion testing. For example, in (Fig. 1D) we show a typical test, where 11 different pieces of ice are all frozen together. Short- and long-length samples were placed within the geometry of the Peltier plate at random locations on the surface to confirm that the measurements did not affect one another. In all these experiments, we used lengths from 0.5 cm to 20 cm. In total, a minimum of five measurements (N = 5) were taken for each length. The height and width of ice were fixed at h = 0.6 cm and w = 1 cm. The ice was frozen at -10 °C. The force required to dislodge the ice was recorded using a force gauge (Nextech DFS500) at a controlled velocity of 74 μm/s (Fig. S1).

To measure the properties of ice interfaces longer than 20 cm, we moved our entire ice-adhesion setup into a walk-in freezer held at either -10°C or -20ºC and 34% RH. We removed the Peltier system, and extended the stage holding the samples by securing a 1.2 m × 0.1 m aluminum plate to our original frame. The whole system was precisely leveled using a bubble level accurate to 1°. A 1 m × 1 cm × 5 mm ($L \times w \times h$) cuvette was fabricated by boring an elongated channel from a piece of stock polypropylene (PP). The sample surface was secured to the Al plate using clamps, and the PP cuvette was placed on top. Deionized water was then poured into the cuvette, and the ice was allowed sufficient time to fully freeze. Once frozen, the force gauge was used to dislodge the PP cuvette near the base of the substrate, at a controlled velocity of 74 μm/s. $\tilde{F}_{ice}$ was recorded as the maximum force at which fracture occurred, and the reported values are the average of a minimum of three measurements.

Aluminum bars of dimensions 1.22 m × 0.025 m × 0.0032 m (McMaster) were used to perform end-loaded cantilever and off-center-loaded beam tests. One of the bars was rendered icephobic after being sanded, cleaned and coated with Silicone B (~0.65 mm thickness). Another bar was coated using a solution of Silicone B and 40 wt% silicone oil (~1 μm thickness) formed in hexane at an overall concentration of 25 mg/mL (for a LIT coating). After curing at room temperature overnight, the bars were taped on the edges using commercial tape and capped at the ends to hold water along a length of 1m. The bars were moved to the walk-in freezer, and rested on lab jacks. The whole system was precisely leveled using a bubble-level accurate to 1°. Deionized water was poured onto the bars, and the ice was allowed sufficient time to fully freeze. Once frozen, the tape and end caps were carefully removed to expose the adhered ice sheet (1.0 m × 0.025 m × 0.008 m). To perform end-

loaded cantilever-beam tests, one end of the Al-ice beam was clamped, while the free end was threaded to the force gauge to apply a force perpendicular to the beam plane. When the ice fractured from the surface, the force was measured and the final deflection of the beam was noted using a digital angle gauge (Wixey), also attached to the free end of the beam. To perform off-center loaded beam tests, the ends of the ice-Al specimen were held and flexed. The minimum deflection to cause the ice-Al interface to fracture (LIT), or the maximum deflection obtainable (Al and icephobic), was analyzed using ImageJ software.

C. Surface analysis. Advancing and receding contact angles were measured using a Ramé-Hart 200 F1 contact-angle goniometer using the standard sessile-drop method (Fig. S2 and S3A). Scanning-electron microscopy (SEM) was performed using a Phillips XL30 FEG. Surface profilometry was performed using an Olympus LEXT interferometer with a step size of 1.25 μm, and an overall scan area of 1.3 × 1.3 mm. The thickness of the samples was measured using either a micrometer (for samples where the coating could be delaminated), or in cross-section using a SEM. An average of four different locations is reported (Fig. S3B).

D. Statistical analysis. In contrast to typical methods where the value of τ_{ice}, resulting from the measurements taken from a single area is calculated, here we report a true interfacial shear strength, $\hat{\tau}$, taken from the slope of the $\tilde{F}_{ice}$ against L fit in the linear (strength-controlled) regime. Often it was ambiguous whether lengths near the transition between the two regimes should be included in the linear fit. For consistency, lengths were included in the linear fit that minimized the overall error in the measurement of $\hat{\tau}$.

For each length of ice, several measurements were taken. For each reported value of $\tilde{F}_{ice}$, the data point is the mean of at least 5 measurements, $\tilde{F}_L$, and the error bar is one standard deviation, Ω_L. The error in $\hat{\tau}$, equivalently the error in the slope, was found using

$$\Omega_\tau = \sqrt{\frac{1}{\Delta}\sum\frac{1}{\Omega_L^2}}, \tag{1}$$

where Δ is given by,

$$\Delta = \sum\frac{1}{\Omega_L^2}\sum\frac{\tilde{F}_L^2}{\Omega_L^2} - \left(\sum\frac{\tilde{F}_L}{\Omega_L}\right)^2. \tag{2}$$

Once the best fit for $\hat{\tau}$ was found using the method described above, $\tilde{F}_{ice}^{cr}$ was determined by averaging the recorded $\tilde{F}_{ice}$ values for all $L > L_c$. The error in the intercept of the best-fit line for $\hat{\tau}$, Ω_{τ_b}, was found using,

$$\Omega_{\tau_b} = \sqrt{\frac{1}{\Delta}\sum\frac{\tilde{F}_L^2}{\Omega_L^2}} \tag{3}$$

The critical interfacial length, L_c, was found from the intersection of the linear fit in the strength-controlled regime ($\hat{\tau}$) and the mean value of $\tilde{F}_{ice}^{cr}$ in the toughness-controlled regime. The error in L_c was then found by perturbing the best-fit line for $\hat{\tau}$ using Ω_τ and Ω_{τ_b}. We computed the maximum and minimum deviations from L_c using $y_{\max} = (m - \delta_m)x + (b - \delta_b)$ and $y_{\min} = (m + \delta_m)x + (b + \delta_b)$, where the best fit for $\hat{\tau}$ is given by the line $y = mx + b$, and the error in the slope and intercept are $\delta_m = \Omega_\tau$ and $\delta_b = \Omega_{\tau_b}$, respectively. $L_c^{\max}$ and $L_c^{\min}$ were then found from the intersection of these deviated lines with $\tilde{F}_{ice}^{cr}$. We then define the error in L_c as $\Omega_{L_c} = \frac{1}{2}(L_c^{\max} + L_c^{\min})$.

E. Outdoor testing of 1m^2 area panels. Aluminum panels with dimensions 1.3m x 1.1m x 0.8 mm were purchased from McMaster and sanded with 1200 Grit sandpaper. A blend of Mold Max STROKE + 40 wt% silicone oil (100 cP, Sigma) was formed in hexane at a concentration of 25 mg/mL. The solution was sprayed onto one side of the panel using an ATD Tools 6903 high-volume-low-pressure spray gun. The coating was allowed to cure at room temperature overnight. The coated panel was bolted to a 2.54 cm thick wooden backing to prevent bending of the panel. A 1m x 1m x 12 cm tall cuvette was made using wood and sealed using Mold Max 40 silicone. The surface, along with a similar, uncoated panel, was taken outdoors and laid facing up during winter in Michigan. Water was poured over the panels and was allowed to freeze gradually overnight. The air temperature fluctuated between -1 °C and -7 °C. Upon freezing, the formed ice had dimensions 1m × 1m × 0.01m. The entire assembly was then rotated 98° from the horizontal (Fig. 3B). The ice sheet fractured from the large LIT PDMS coated specimen solely by its own weight. Ice frozen to the same uncoated Al sheet remained adhered (Movie S5).

F. Ice-cube-tray experiments. Commercial ice-cube trays were purchased from Kitch. A blend of Mold Max STROKE + 40 wt% silicone oil (100 cP, Sigma) was formed in hexane at a concentration of 25 mg/mL. 30 mL of solution was sprayed onto the ice cube tray using an ATD Tools 6903 high-volume-low-pressure spray gun. The coating was allowed to cure at room temperature overnight. To fabricate an identical geometry of ice-cube tray out of an icephobic material, Vytaflex 40 (Smooth-On Inc.) was mixed with 15 wt% safflower oil (high linoleic, Jedwards International) without dilution *(14)*. Once homogeneous, the prepolymer mixture was poured over the back of the tray to cast a replicate mold. The icephobic rubber was allowed to cure at room temperature overnight. We poured water, dyed blue for contrast, into both a coated (icephobic and LIT coating) and an uncoated polypropylene tray and left them in a -20 °C freezer for 72 hours. The force required to detach the ice from the tray was measured by clamping three corners of the inverted iced tray and applying a normal force on the fourth corner with a force gauge. For comparison, the force at which 50% or more of the ice cubes detached was recorded for the uncoated and LIT tray (Movie S4).

G. Ice adhesion measurements under different environmental conditions. To investigate the dependence of ice adhesion on different ice forming temperatures and conditions, we conducted

additional experiments to measure the critical force per unit width ($\tilde{F}_{ice}^{cr}$), and the corresponding interfacial strength ($\hat{\tau}$), and interfacial toughness (Γ) for two different samples (polypropylene and low interfacial toughness PDMS) at three different temperatures (-20ºC, -10ºC and -5ºC). Additionally, at the same temperature (-20ºC), we also conducted additional experiments where the ice was formed either by cooling on top of a Peltier plate or by cooling in a large freezer (where the entire volume of the freezer was at this low temperature). From the data (Fig. S4) the values of $\tilde{F}_{ice}^{cr}$, $\hat{\tau}$, and Γ for both the LIT-PDMS and polypropylene appear to be independent of temperature within the range studied. Moreover, these interfacial properties were also statistically equivalent for the two different ice-formation conditions (Peltier vs freezer) tested at -20 °C.

H. Verification that the LIT PDMS coatings did not fail cohesively during ice removal. To investigate whether the LIT PDMS coatings failed cohesively upon de-icing, a 10 × 1 cm ice block was debonded from the coating within our typical ice adhesion test on a Peltier plate. The ice block was then melted, and the melt water analyzed using Fourier-transform infrared (FTIR) spectroscopy. For the FTIR analysis we used a Thermo Scientific Nicolet 6700 FTIR spectrometer with ATR (diamond crystal) over a frequency range of 400 - 4,000 cm^{-1} (Fig. S5A). Pure water was used as the negative control. As a positive control, 0.3 mg of the LIT PDMS coating was deliberately added to 60 mg of pure water. The LIT PDMS material was also analyzed.

The melt water, negative and positive controls were also analyzed using a Discovery Differential Scanning Calorimeter (DSC; TA Instruments) under a nitrogen atmosphere, with a heating rate of 5°C/min, over a temperature range from -80 °C to 100 °C (Fig. S5B). A peak at 0°C corresponded to the freezing of water. A peak at -40 °C corresponded to the crystallization of a fraction of the silicone oil present in the LIT PDMS coating *(47)*. A clear signature of silicone oil crystallization was observed for the positive control and LIT PDMS samples, but not the melt water. The absence of any remnant LIT PDMS material within the melt water indicated that the coating was not failing cohesively.

Section 2. Supplementary Discussion

A. Cohesive-zone model. In this section we summarize key concepts for delamination of a coating from a substrate from the perspective of a cohesive-zone model. In the subsequent section, we provide a simple analytical model to make these points more accessible.

The bonding across an interface may be characterized by two distinct physical properties: the strength (N/m^2) (maximum value of the bonding tractions), and the toughness (J/m^2) (area under the traction-displacement curve for an interface) *(18)* (Fig. S6). For the interface between ice and a substrate, we refer to the interfacial adhesion strength, $\hat{\tau}$, and the interfacial toughness, Γ. The field of interfacial-fracture mechanics has focused on the role of interfacial toughness, rather than adhesive strength, as an important fracture parameter, based on the original insight of Griffith (*10*). However, work in the field of cohesive-zones has emphasized that both parameters need to be considered when addressing issues of scale on fracture / adhesion problems *(18, 20, 22)*.

Typically, adhesion is a mixed-mode problem *(19, 20)*, involving both shear (mode-II) and normal (mode-I) components. We present the basic concepts of adhesion from the perspective of it being controlled by shear. Whether strength or toughness controls the fracture of any interface depends on the length of the interface compared to the nominal cohesive length, $\zeta = \bar{E}\Gamma/\hat{\tau}^2$, where $\bar{E}$ is the effective modulus of the ice, $\hat{\tau}$ and Γ are the interfacial shear strength and toughness *(18, 19, 22)*. If the bonded length is much larger than ζ, the toughness of the interface controls fracture. If the bonded length is much smaller than this quantity, then the strength controls fracture. Here we show that this general rule for fracture holds true for the interface between a substrate and ice. For a fixed value of $\hat{\tau}$, a strength-based argument indicates that the force per unit width to remove a block of adhered ice is given by

$$\tilde{F}_{ice} = F / w = \hat{\tau} \times L \quad , \tag{4}$$

where, L and w are the length and width of the ice interface, parallel and perpendicular to the direction of the applied force, respectively. This assumes that the stresses are uniform along the interface, and that any initial de-bond, a, is much less than L. Throughout this work, we discuss the two-dimensional case, and always denote the fracture force per unit width as $\tilde{F}_{ice}$.

On the other hand, the ice/material interface may fracture by the propagation of a crack along the interface (Movie S1). This would occur if the bonded length is much larger than ζ, so that the toughness of the interface controls fracture. This failure occurs when the interface is large enough that the interfacial stresses are no longer uniform along the interface but are instead concentrated near the tip of the crack. Such an interfacial crack will advance if the potential energy of the system decreases by an amount greater than the increase in energy associated with the creation of new surfaces *(21)*. In this case, the force (per unit width) required to de-bond the interface between the ice and substrate is of the form (21, 27-29, *44*),

$$\tilde{F}_{ice} = \sqrt{2\bar{E}\Gamma h} \, , \tag{5}$$

where h is the thickness of the ice layer. In this limit, the layer thickness, not the ligament length, controls the debonding process. For geometrically similar materials, this leads to a dependence of *apparent* shear strength ($\tau_{ice} = \tilde{F}_{ice} / L$) on ligament length.

An important concept to appreciate, which distinguishes analyses for debonding layers different from other types of fracture problems, is the fact that it is the layer thickness, h, not the debond (crack) length, a, that controls the energetics of crack propagation. Only when $a < h$ does a enter the expression for the energy-release rate, affecting the results for linear-elastic fracture mechanics (LEFM), which corresponds to $\zeta \Rightarrow 0$. However, for systems where the interfacial strength is small enough for cohesive-zone models to be useful for describing the interface, ζ is generally large enough to make these small-crack results from LEFM irrelevant, leaving h, L, and ζ the length parameters that control fracture. This is the reason why debonding of interfaces with relatively large values of ζ are relatively flaw-insensitive, as seen from the consistency of the experimental results given in this paper. This point will also be made by the results of the analysis of the next section, where the strength and toughness limits arise naturally from a cohesive-zone analysis in which the fracture load is totally insensitive to any assumed initial flaw.

The fracture of an interface is controlled by the lowest of the loads given by Eqns. (4) and (5) *(20)*. This means that the strength for small structures (within the strength-controlled regime) will increase linearly with L, until a critical length, L_c, is reached. Beyond L_c, toughness dominates interfacial fracture, the failure load becomes independent of L, and τ_{ice} will decrease as the interfacial length increases (Fig. 1). In the toughness-controlled regime, the force required for detachment becomes independent of the length of the adhered ice for a fixed value of h. From this asymptotic value, $\tilde{F}_{ice}^{cr}$, the interfacial toughness can be calculated from *(27-29)*

$$\Gamma = \frac{(\tilde{F}_{ice}^{cr})^2}{2E_{ice}h} \ , \tag{6}$$

where E_{ice} is the elastic modulus of ice (≈ 8.5 GPa) (*45*). Whether an icephobic material (low $\hat{\tau}$), or a LIT material (low Γ) will require less force to detach adhered ice will depend on how the interfacial length, L, compares to L_c. L_c for a material may be found when the force of fracture for the strength (Eq. 4) and toughness (Eq. 6) regimes are equated:

$$L_c \approx 1.4\sqrt{\bar{E}\Gamma h / \hat{\tau}^2} \ . \tag{7}$$

Note that decreasing $\hat{\tau}$ in Eq. (7) increases L_c, and, thus, extremely long interfacial lengths are necessary to observe toughness-controlled fracture between ice and icephobic materials ($\hat{\tau}$ << 100 kPa). In contrast, it was possible to observe a toughness-controlled regime of fracture for all thirteen plastics we tested (L_c ~ 3.5 cm – 10 cm) (Figs. S7-S12).

B. Analysis of strength and toughness regimes using cohesive zone analysis.

In the analyses that follow, the ice is assumed to have a modulus $\bar{E}$, the substrate is assumed to be rigid, and only shear tractions from the cohesive layer are considered. Furthermore, the stresses in the ice are assumed to be uniform at each section (see Fig. S13).

The analysis is conducted for two simple types of cohesive law. The first is a simple Dugdale type of bonding, where the shear stress transmitted by the cohesive layer has a constant value of $\hat{\tau}$ until a critical displacement between the ice and substrate of u_c, at which separation occurs. This provides a simple model for slip at the interface between the ice and coating, with a toughness of $\Gamma = \hat{\tau} u_c$. The second model is a linear cohesive law, where the cohesive law is of the form, $\tau = ku$, where k is the shear stiffness of the cohesive law. De-bonding is assumed to occur at a critical displacement u_c, corresponding to a cohesive strength of $\hat{\tau} = ku_c$, and a toughness of $\Gamma = \hat{\tau} u_c / 2$. We suggest in the manuscript that the coating can be included in the cohesive layer, so that the shear stiffness can be represented as $k = G/t$, where G is the shear modulus of the coating, and t is its thickness. However, for the purposes of the present analysis, we characterize the cohesive law in terms of Γ and $\hat{\tau}$, so that $k = \hat{\tau}^2 / 2\Gamma$.

Dugdale Model

The analysis proceeds by considering an element of length δx, in a layer of ice of thickness h and total length L (Fig. S13), subject to a compressive applied load P at one end ($x = 0$). At the interface between the ice and rigid substrate there is a shear stress $\tau(x)$, which for the Dugdale model is a constant of $\tau(x) = \hat{\tau}$. Equilibrium of the element results in the equation

$$h \frac{\partial \sigma(x)}{\partial x} = -\hat{\tau} \quad . \tag{8}$$

In addition, the constitutive relationship for the ice gives a relationship between the local compressive stress, $\sigma(x)$, and the local displacement relative to the substrate, $u(x)$:

$$\sigma(x) = -\bar{E} \frac{\partial u(x)}{\partial x} \quad . \tag{9}$$

The boundary condition for $x = 0$ is $\sigma(0) = P/h$. Combining Eqns. (8) and (9) gives the governing equation for $u(x)$:

$$\frac{\partial^2 u(x)}{\partial x^2} = \frac{\hat{\tau}}{\bar{E}h} \quad , \tag{10}$$

within the region of slip, $x < l_s$, for which $u(x) > 0$. Beyond the slip region, $x > l_s$, $u(x) = 0$, since we assume the substrate is rigid.

The solution to Eqn. (10), within the slip region is

$$u(x) = \frac{\hat{\tau}x^2}{2\bar{E}h} - Ax + B \quad . \tag{11}$$

This can be solved with boundary conditions $u'(0) = -P/Eh$, and $u(l_s) = 0$ at the transition from slip to no slip if, $l_s < L$ (partial slip). This gives a result that the relative slip between the ice and substrate is given by

$$\begin{aligned} u(x) &= \frac{\hat{\tau}x^2}{2\bar{E}h} - \frac{Px}{\bar{E}h} + \frac{P^2}{2\bar{E}h\hat{\tau}} \qquad x < l_s \\ u(x) &= 0 \qquad\qquad\qquad\qquad\qquad x > l_s \end{aligned} \quad , \tag{12}$$

with $l_s = P/\hat{\tau}$. The maximum load, P_f, that can be supported before failure of the interface occurs can be found by setting $u(0)$ to its maximum value of $u_c = \Gamma/\hat{\tau}$. For the partial-slip condition, for which $l_s < L$,

$$P_f = \sqrt{2\Gamma Eh} \tag{13}$$

This is the result for the toughness-limited regime.

If there is full slip along the interface ($L = l_s$), then the requirement to maintain equilibrium dictates that the maximum load that can be applied is given by

$$P_f = \hat{\tau}L \tag{14}$$

This is the result for the strength-limited regime.

These results can be summarized as a plot of how the maximum load varies with L (Fig. S14)

Linear Cohesive Law

The starting equation for this analysis is the equation for equilibrium:

$$h\frac{\partial\sigma(x)}{\partial x} = -ku(x)\,. \tag{15}$$

When combined with the constitutive equation (Eqn. 9, above), the governing differential equation becomes

$$\frac{\partial^2 u(x)}{\partial x^2} = \frac{k}{\bar{E}h} u\left(x\right) \quad . \tag{16}$$

The solution to this equation is

$$u(x) = Ae^{\omega x} + Be^{-\omega x} \tag{17}$$

where,

$$\omega = \sqrt{\frac{k}{\bar{E}h}} = \frac{\hat{\tau}}{\sqrt{2\Gamma\bar{E}h}} \tag{18}$$

The boundary conditions for this problem are now $u'(0) = -P / \bar{E}h$, and $u'(L) = 0$. The solution for the displacement is given by

$$u\left(x\right) = \frac{P}{\sqrt{\bar{E}hk}}\left[\frac{1}{1-e^{-2\omega L}}\right]\left[e^{-2\omega L}e^{\omega x} + e^{-\omega x}\right] \tag{29}$$

The debond starts to propagate when $u(0) = u_c$. This gives a value for the maximum load the ice layer can support as

$$P_f = \sqrt{2\Gamma\bar{E}h}\,\frac{1-e^{-2\omega L}}{1+e^{-2\omega L}} \tag{20}$$

As the debond starts to propagate and develop a crack of length a, the bonded length L decreases accordingly, and (under displacement control), the load drops as given by Eqn. (20) until complete failure has occurred. Notice, that the analysis is totally unchanged for values of $a \neq 0$, confirming that the presence of a crack has no influence on this analysis. Asymptotic results for relatively short and relatively long bonded lengths can be found from the limiting results of $L \Rightarrow 0$, and $L \Rightarrow \infty$. When $L \Rightarrow \infty$, Eqn. (20) becomes

$$P_f = \sqrt{2\Gamma\bar{E}h} \tag{21}$$

This is the result that one can obtain from linear-elastic fracture mechanics for the propagation of an interface with a toughness Γ. When $L \Rightarrow 0$, Eqn. (20) becomes

$$P_f = \omega L\sqrt{2\Gamma\bar{E}h} \quad . \tag{22}$$

Substituting the value of ω from Eqn. (18), one obtains the strength limit of

$$P_f = \hat{\tau}L \tag{23}$$

Again, both the strength-controlled and toughness-controlled limits evolve from a simple cohesive-zone model, as they did with the Dugdale model. In particular, it should be noted that the geometry of a layer on a substrate has the special nature that the characteristic length scale for fracture mechanics is the layer thickness, rather than a crack length, so the LEFM result evolves without recourse to any assumptions about pre-existing flaws.

A plot of the load required to cause separation of the ice from the substrate is shown in figure S15. On this figure, the load is compared to that arising from the Dugdale (slip) analysis given above. It will be seen that for short and long bonded interfaces, the two distinct solutions from the Dugdale model (the strength and toughness regimes) emerge as asymptotes.

C. Design equation for modulating ice-coating interfacial toughness using a cohesive-zone analysis. Γ represents the energy required to de-bond an interfacial area and is equal to the area under the traction-separation curve *(19)* (Fig. S6). With a compliant coating between the ice and substrate, the deformation of the coating can be considered to be an integral part of the traction-separation curve. In this way, one can treat a coating as part of the interphase between the ice and the underlying substrate, and model the entire interphase with a cohesive-zone analysis *(19)*. If one assumes the coating behaves in a linear-elastic fashion, and the critical shear stress for failure of the ice-coating interface is $\hat{\tau}$, the shear displacement across the coating at fracture can then be found as $\delta_c = \gamma_c t = \hat{\tau} t / G$, where G is the shear modulus of the coating, γ_c is the shear strain when the shear stress equals $\hat{\tau}$, and t is the coating thickness. The interfacial toughness can then be approximated as,

$$\Gamma \approx \frac{\hat{\tau}^2 t}{2G} \quad . \tag{24}$$

D. Reconciling interfacial slippage with interfacial toughness

In our previous work we derived a framework to predict the ice adhesion strength of an oil-filled elastomer, knowing only properties of the elastomer and oil *(35)*. The framework can be written as,

$$\frac{\tau_{oil}}{\tau_{no-oil}} = (1-\phi_{oil})^{5/3}(1-\alpha\phi_{oil}/\phi_{oil}^{\max}) \tag{25}$$

Here the ice adhesion strength of the dry and oil-filled elastomers are denoted τ_{no-oil} and τ_{oil}, respectively. The amount of oil used to plasticize the rubber is ϕ_{oil}, and the solubility limit of that particular oil in that specific elastomer is $\phi_{oil}^{\max}$. α was a proportionality constant found to be $\alpha \approx 0.7$. Because some of the LIT systems developed in this work are fabricated from plasticized elastomers, it is interesting to try and reconcile the effects of interfacial slippage, the mechanism responsible for the above model, with interfacial toughness. An additional set of experiments was conducted with the LIT PDMS (Silicone B plasticized with 40 wt% silicone oil and a thickness of 1 - 2 microns) and a similar formulation without plasticization: Silicone B, no

oil, thickness of 1 - 2 microns. The results can be seen in Figure S16. This non-plasticized Silicone B is denoted as LIT because the resultant interfacial toughness is $\Gamma = 0.69 \pm 0.14$ J/m^2.

In the main manuscript we derived an approximation to the interfacial toughness, $\Gamma \approx \hat{\tau}^2 t / 2G$, where t and G are the thickness and shear modulus of the coating, and $\hat{\tau}$ is the interfacial shear strength with ice. If we use a similar nomenclature as above for surfaces with and without oil, and assume that the two elastomers have the same thickness, we obtain

$$\frac{\Gamma_{oil}}{\Gamma_{no-oil}} = \frac{\frac{\hat{\tau}_{oil}^2 t_{oil}}{2G_{oil}}}{\frac{\hat{\tau}_{no-oil}^2 t_{no-oil}}{2G_{no-oil}}} = \left(\frac{\hat{\tau}_{oil}}{\hat{\tau}_{no-oil}} \right)^2 \left(\frac{G_{no-oil}}{G_{oil}} \right) . \quad (26)$$

Recognizing from our previous work *(20)* that $(1-\phi_{oil})^{5/3}$ is equal to (G_{oil}/G_{no-oil}), and that τ_{oil} and τ_{no-oil} in the previous work are identical to $\hat{\tau}_{oil}$ and $\hat{\tau}_{no-oil}$ in the present work, Eqns. (25) and (26) can be combined to give

$$\frac{\Gamma_{oil}}{\Gamma_{no-oil}} = (1-\phi_{oil})^{5/3}(1-\alpha\phi_{oil}/\phi_{oil}^{\max})^2. \quad (27)$$

Silicone B has a maximum silicone oil (100 cP) solubility around $\phi_{oil}^{\max} \approx 0.95$. Using our experimentally calculated value for Γ_{no-oil} from above would yield $\Gamma_{oil} = 0.14$ J/m^2. From the main manuscript we found $\Gamma_{oil} = 0.12 \pm 0.03$ J/m^2 for our LIT PDMS (LIT Plasticized Silicone B in Figure S16). For the LIT PVC system ($\phi_{oil} = 0.5$), $\Gamma_{no-oil} = 1.8$ J/m^2 and $\phi_{oil}^{\max} \approx 0.9$ (*35*), resulting in a predicted $\Gamma_{oil} = 0.20$ J/m^2. The LIT PVC from the main manuscript exhibited $\Gamma_{oil} = 0.27 \pm 0.07$ J/m^2. Thus, the interfacial toughness values observed for plasticized polymers are not inconsistent with our previous understanding of surfaces exhibiting interfacial slippage, at least for those two systems where the deformation of the compliant coatings contribute significantly to the toughness of the interface.

E. Ice-cube tray experiment results. To highlight the advantage of LIT materials, we coated an ice cube tray with our LIT PDMS material. We poured water, dyed blue for contrast, into both a coated and uncoated polypropylene tray and left them in a -20 °C freezer for 72 hours. Upon flipping the trays upside-down, almost all the ice cubes fell from the LIT PDMS-coated tray, solely under the force of gravity. All the ice cubes remained well-adhered to the uncoated tray (Fig. S17). The remaining ice cubes required a 67% less force for release from the LIT tray (11 ± 3 N) as compared to the uncoated tray (34 ± 11 N) (see section 1F). We also molded this tray from an extremely icephobic material (Vytaflex 40 + 15 wt% safflower oil, $\hat{\tau} \approx 4$ kPa). Similar to the uncoated tray, the ice cubes did not release from the icephobic material, even though the ice adhesion strength was an order of magnitude lower than the LIT PDMS. A minimum of three independent experiments were conducted. Thus, even for complex geometries with three-dimensional ice interfaces, LIT materials display promising anti-icing capabilities.

Section 3. Supplementary Figures

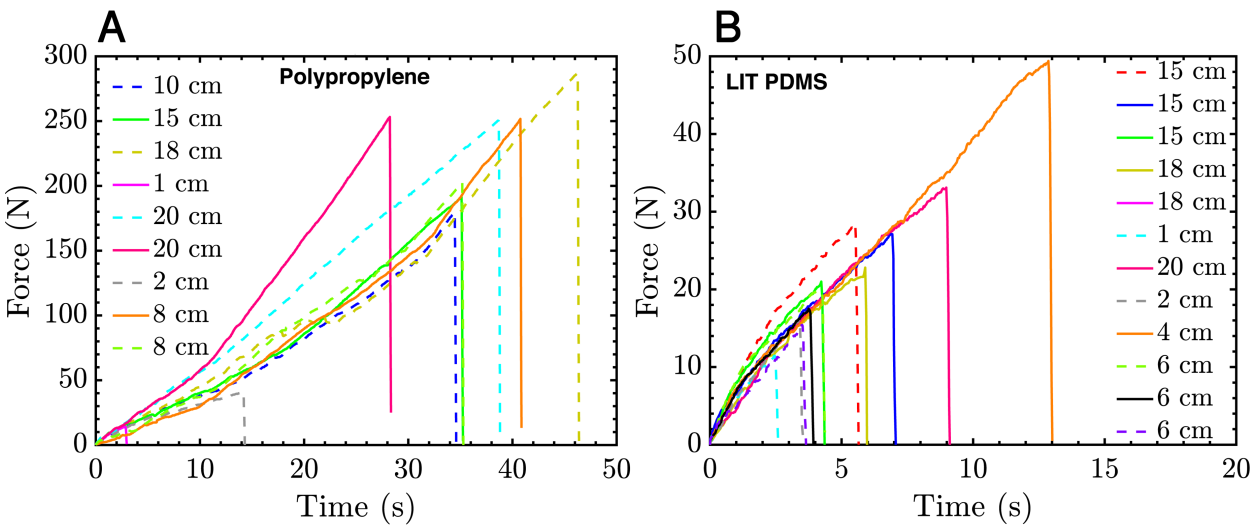

Figure S1. Force-time curves for (A) polypropylene (L_c = 3.6 ± 0.7 cm) and (B) LIT PDMS (L_c = 6.7 ± 3.2 cm).

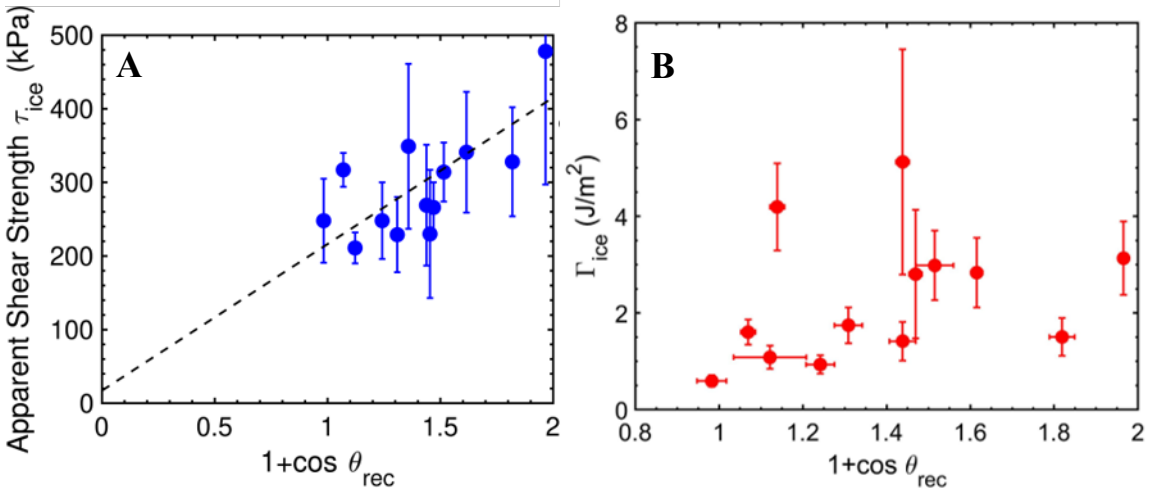

Figure S2. The effect of surface energy. (A) Previous work has shown that the work of adhesion ($W_a \propto 1+\cos\theta_{rec}$) is proportional to the ice adhesion strength *(2)*. We observed this trend for the 13 different plastics tested. **(B)** However, we found no sole correlation between the work of adhesion and Γ, indicating that hydrophobicity mainly affects the strength-controlled regime of fracture. Error bars denote 1 standard deviation (N ≥ 5).

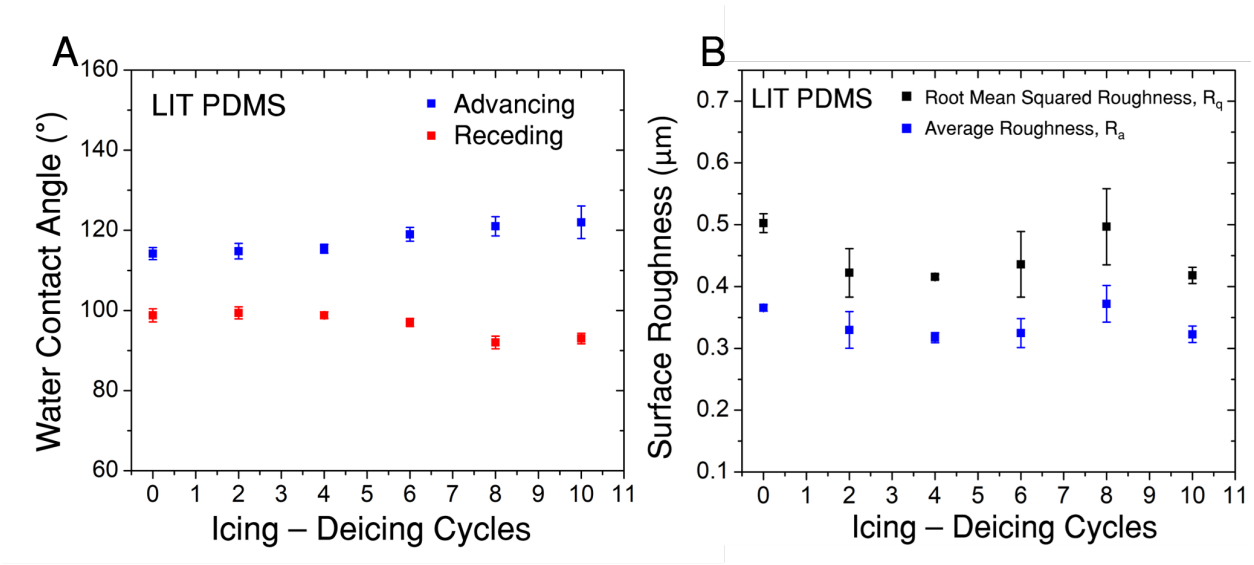

Figure S3. Effect of repeated icing-deicing cycles on surface properties. **(A)** Data for advancing and receding contact angles with water on the LIT – PDMS surface after 10 icing – dicing cycles. **(B)** Surface roughness measurements on the LIT – PDMS surface (both root mean square and average roughness) during 10 icing-deicing cycles. There is no significant change in the advancing contact angles, receding contact angles, or the surface roughness after the 10 icing–deicing cycles. The LIT coating is thus not getting damaged (evident from insignificant surface roughness change) or delaminating (absence of drastic changes in the contact angles) during these icing-deicing cycles. Also see Table S1. Error bars denote 1 standard deviation ($N \geq 4$).

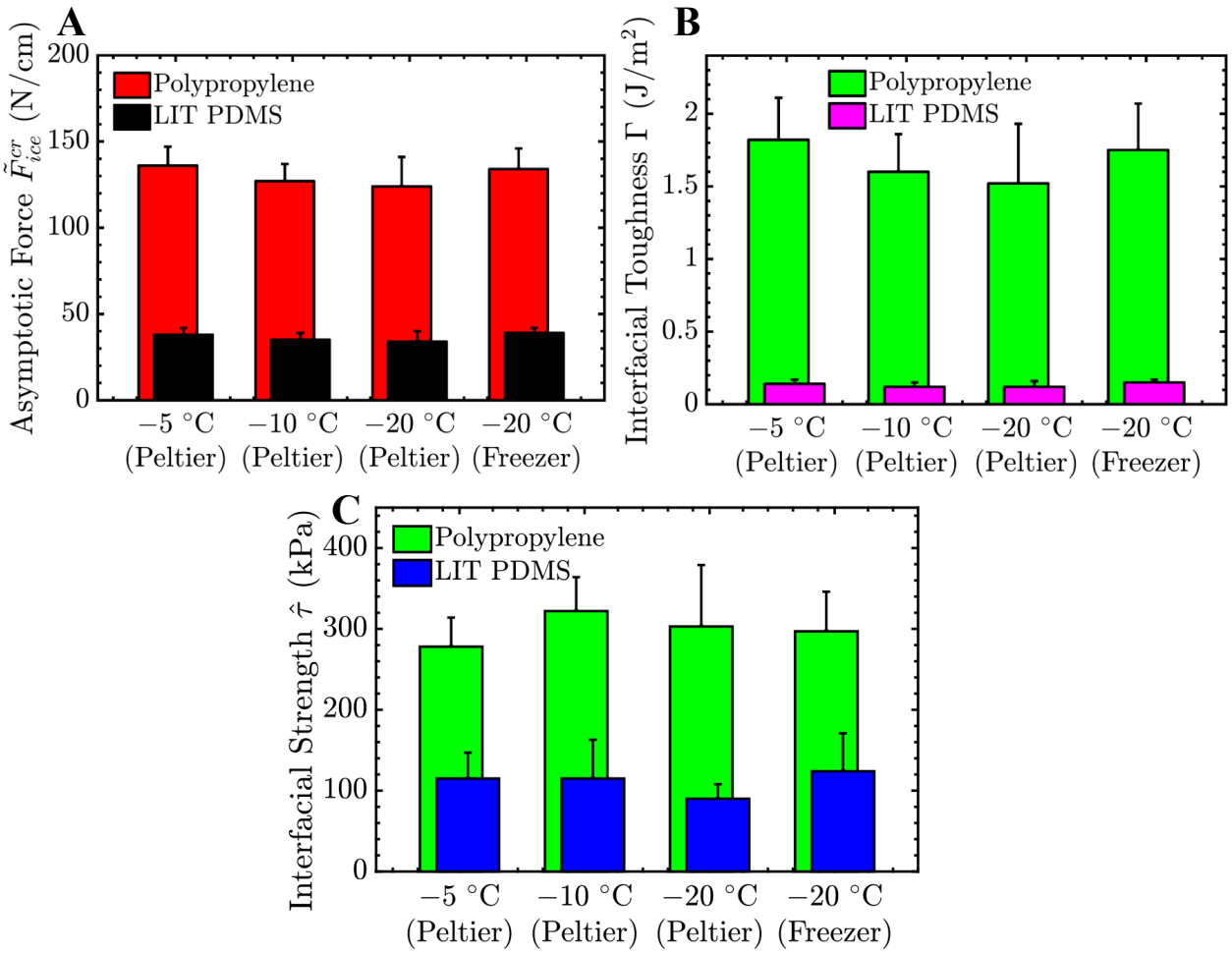

Figure S4. Ice adhesion measurements at different freezing conditions. (A) Critical force per unit width ($\tilde{F}_{ice}^{cr}$), **(B)** interfacial toughness (Γ), and **(C)** interfacial strength ($\hat{\tau}$) measurements for two different samples (polypropylene and low interfacial toughness PDMS) at three different temperatures (-20 ºC, -10 ºC and -5 ºC). Additionally, at the same temperature (-20 ºC), the ice was formed either by cooling on top of a Peltier plate or by cooling in a large freezer (where the entire volume of the freezer was at this low temperature). The values of $\hat{\tau}$, $\tilde{F}_{ice}^{cr}$ and Γ for both the LIT-PDMS and polypropylene appear to be independent of temperature within the range studied. Moreover, these interfacial properties were also statistically equivalent for the two different ice-formation conditions (Peltier vs freezer) tested at -20 °C. Error bars denote 1 standard deviation ($N \geq 5$).

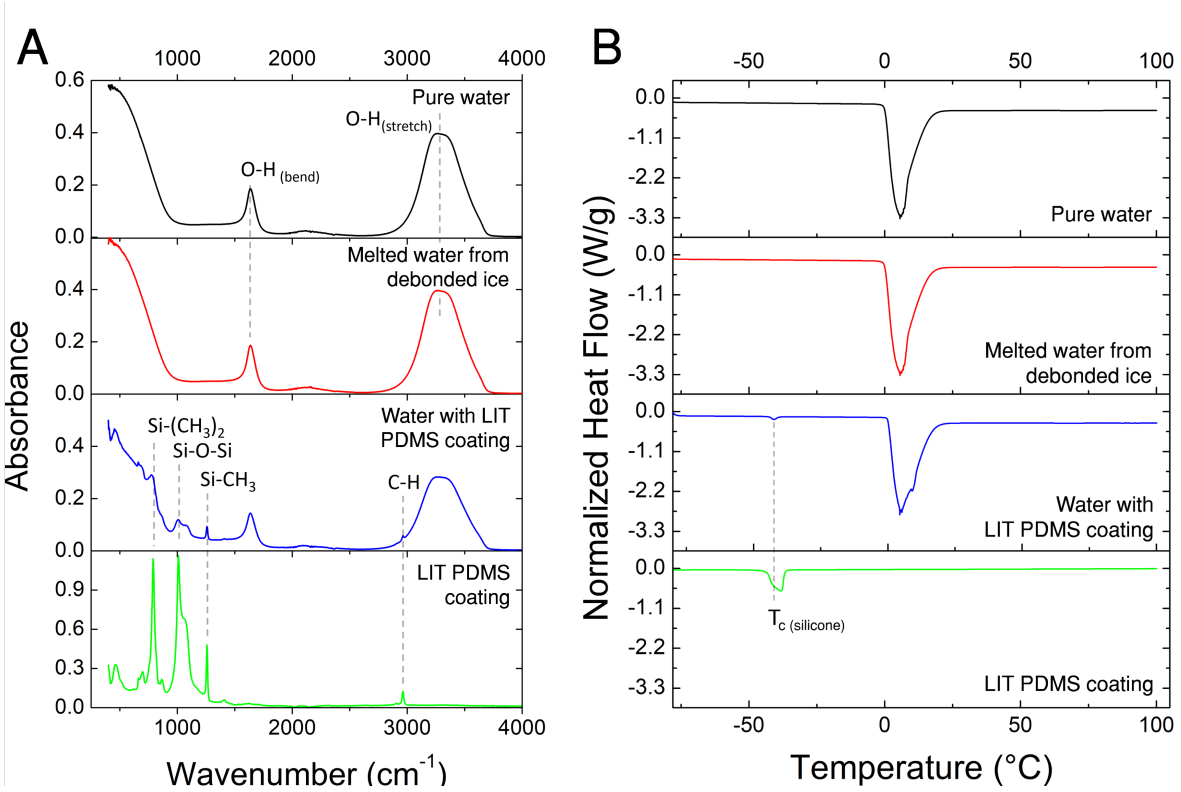

Figure S5. Confirmation that the LIT PDMS coating does not fail cohesively upon ice removal. Ice debonded from a LIT PDMS specimen was melted and analyzed for remnants of the coating via **(A)** FTIR spectroscopy and **(B)** Differential Scanning Calorimetry – DSC *(23)*. Pure water and water deliberately contaminated with the LIT PDMS sample were used as the negative and positive control, respectively. LIT PDMS was also analyzed separately for comparison. **(A)** shows absorbance curves for vibrational peaks for O-H stretching (3262 cm^{-1}) and bending (1635 cm^{-1}) for water and the melt water from the debonded ice specimen. The melt water lacked bond vibrational peaks for Si-$(CH_3)_2$ (787 cm^{-1}), Si-O-Si (1007 cm^{-1}), Si-CH_3 (1258 cm^{-1}), and C-H (2962 cm^{-1}). These peaks would be present if there were remnants of the LIT PDMS coating present within the melt water, as a result of cohesive failure of the coating. These peaks were observed for the positive control and the LIT PDMS material. **(B)** shows normalized heat flow curves for pure water, melt water and the positive control. Clear signatures (valleys in the heat flow curve) associated with the crystallization of some fraction of the silicone oil were observed for the positive control, as well as the LIT PDMS material at a temperature (T_c) around -40 °C *(47)*. This signature was absent in the melt water.

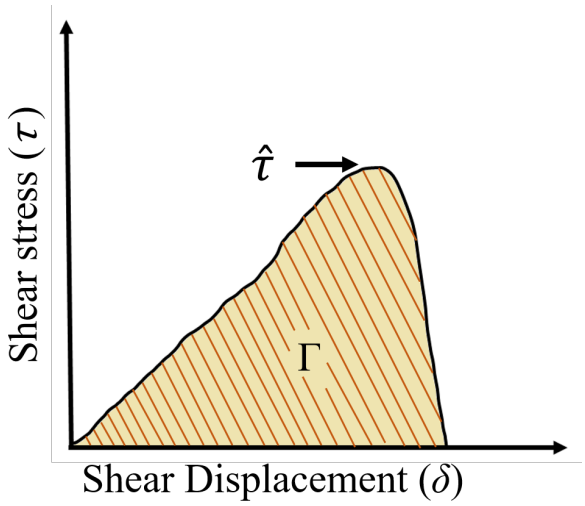

Figure S6. Traction-separation law for an ice-coating interface. From a cohesive-zone perspective, one can consider the toughness of an interface to be given by the area under the force-displacement curve for the tractions across the interface *(18,19)*. The interfacial cohesive strength is the maximum value of the shear tractions, $\hat{\tau}$. It is also possible to incorporate the deformation of the coating into the cohesive law. If the deformation of the coating provides a dominant contribution to the cohesive law, and it behaves in a linear-elastic fashion, the toughness can be estimated by $\Gamma \approx \hat{\tau}^2 t / 2G$, where G is the shear modulus and t is the thickness of the coating.

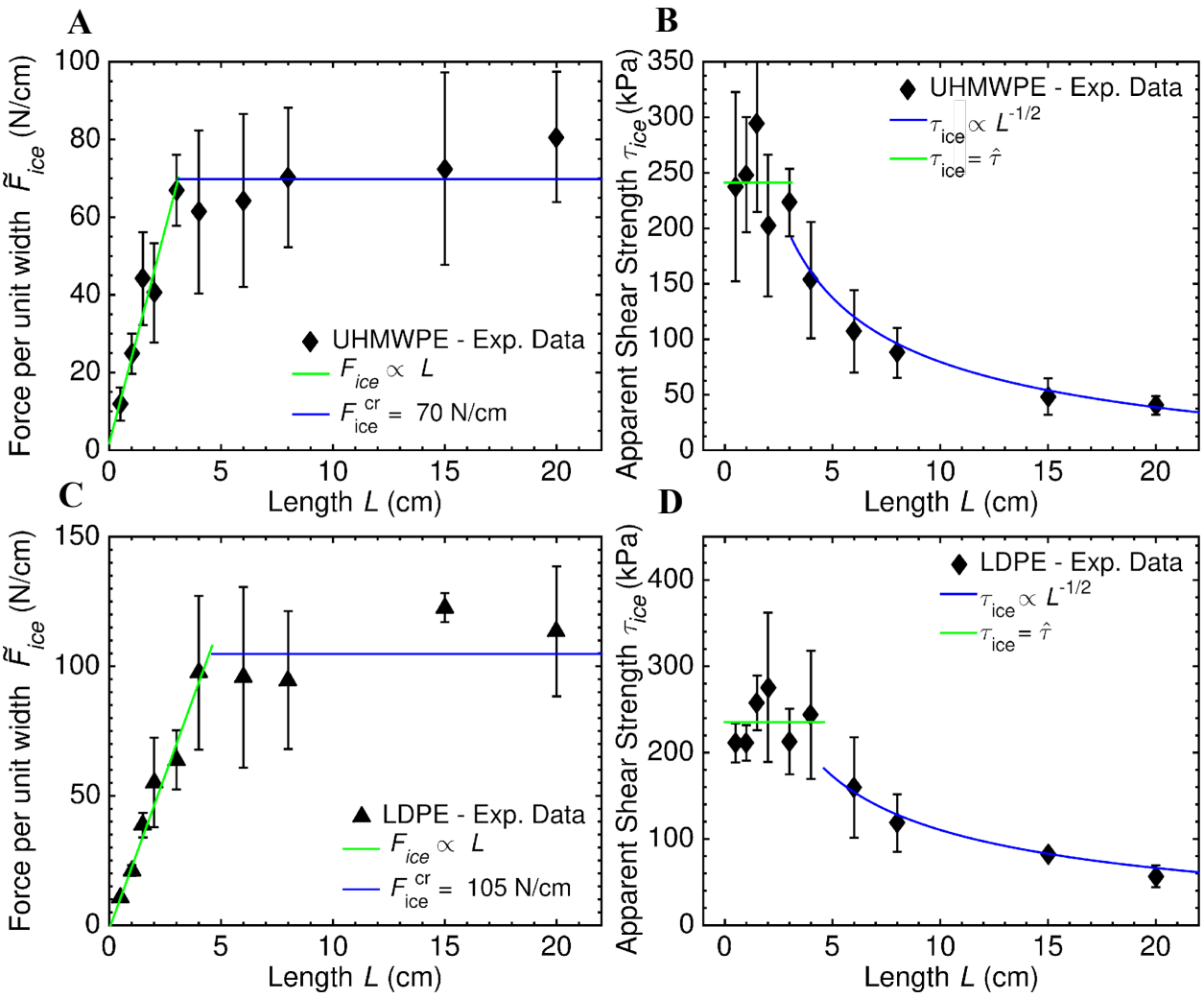

Figure S7. Fracture of ice from UHMWPE and LDPE. (A) The force per unit width required to detach adhered ice from UHMWPE (1.6 mm thick). **(B)** The apparent ice-adhesion strength of UHMWPE. After $L_c = 3.8$ cm, the force became constant and τ_{ice} began to decrease. At $L = 20$ cm, $\tau_{ice} = 49 \pm 4.9$ kPa. **(C)** The force per unit width required to detach ice from LDPE (1.6 mm thick). **(D)** The apparent ice-adhesion strength of LDPE. After $L_c = 4.6$ cm, the force became constant and τ_{ice} began to decrease. At $L = 20$ cm, $\tau_{ice} = 52 \pm 5.9$ kPa. Error bars denote 1 standard deviation ($N \geq 5$).

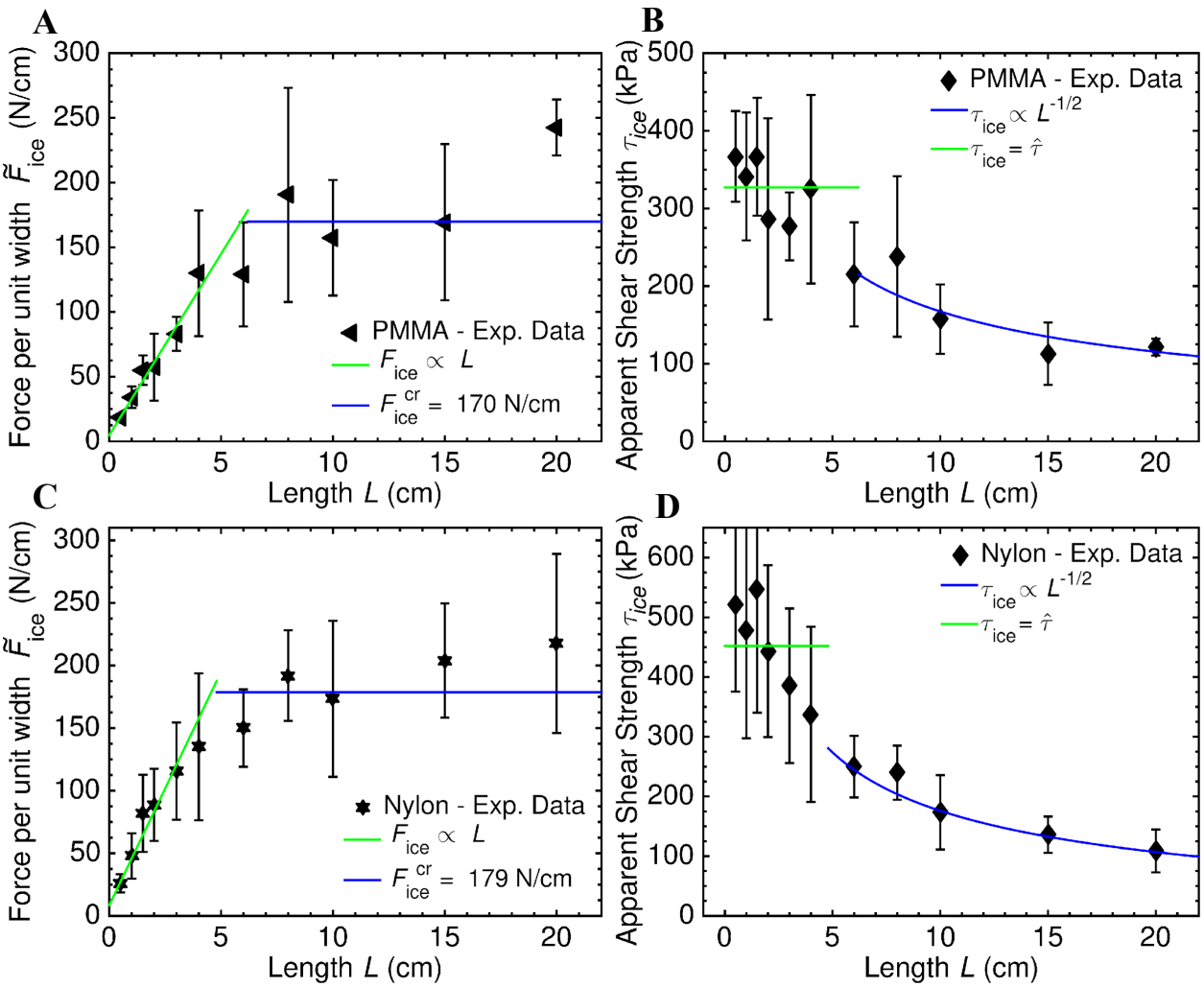

Figure S8. Fracture of ice from PMMA and Nylon. (A) The force per unit width required to detach adhered ice from PMMA. **(B)** The apparent ice-adhesion strength of PMMA (1.6 mm thick). After $L_c = 6.2$ cm, the force became constant and τ_{ice} began to decrease. At $L = 20$ cm, $\tau_{ice} = 121 \pm 11$ kPa. **(C)** The force per unit width required to detach ice from Nylon (1.6 mm thick). **(D)** The apparent ice-adhesion strength of Nylon. After $L_c = 4.8$ cm, the force became constant and τ_{ice} began to decrease. At $L = 20$ cm, $\tau_{ice} = 89 \pm 11$ kPa. Error bars denote 1 standard deviation ($N \geq 5$).

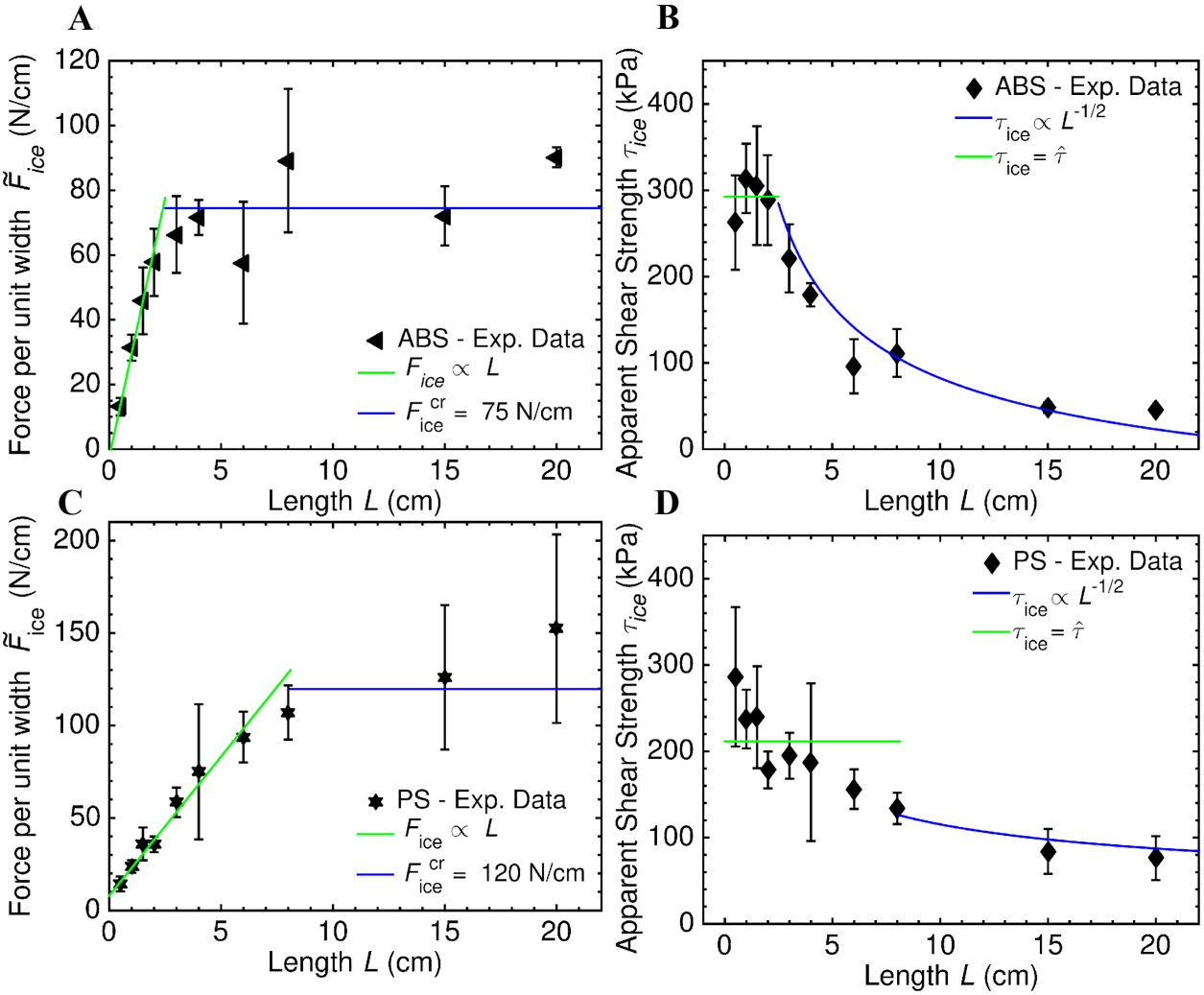

Figure S9. Fracture of ice from ABS and PS. (A) The force per unit width required to detach adhered ice from ABS. **(B)** The apparent ice-adhesion strength of ABS (1.6 mm thick). After $L_c = 10$ cm, the force became constant and τ_{ice} began to decrease. At $L = 20$ cm, $\tau_{ice} = 86 \pm 30$ kPa. **(C)** The force per unit width required to detach ice from PS. **(D)** The apparent ice-adhesion strength of PS (1.6 mm thick). After $L_c = 8.1$ cm, the force became constant and τ_{ice} began to decrease. At $L = 20$ cm, $\tau_{ice} = 76 \pm 25$ kPa. Error bars denote 1 standard deviation ($N \geq 5$).

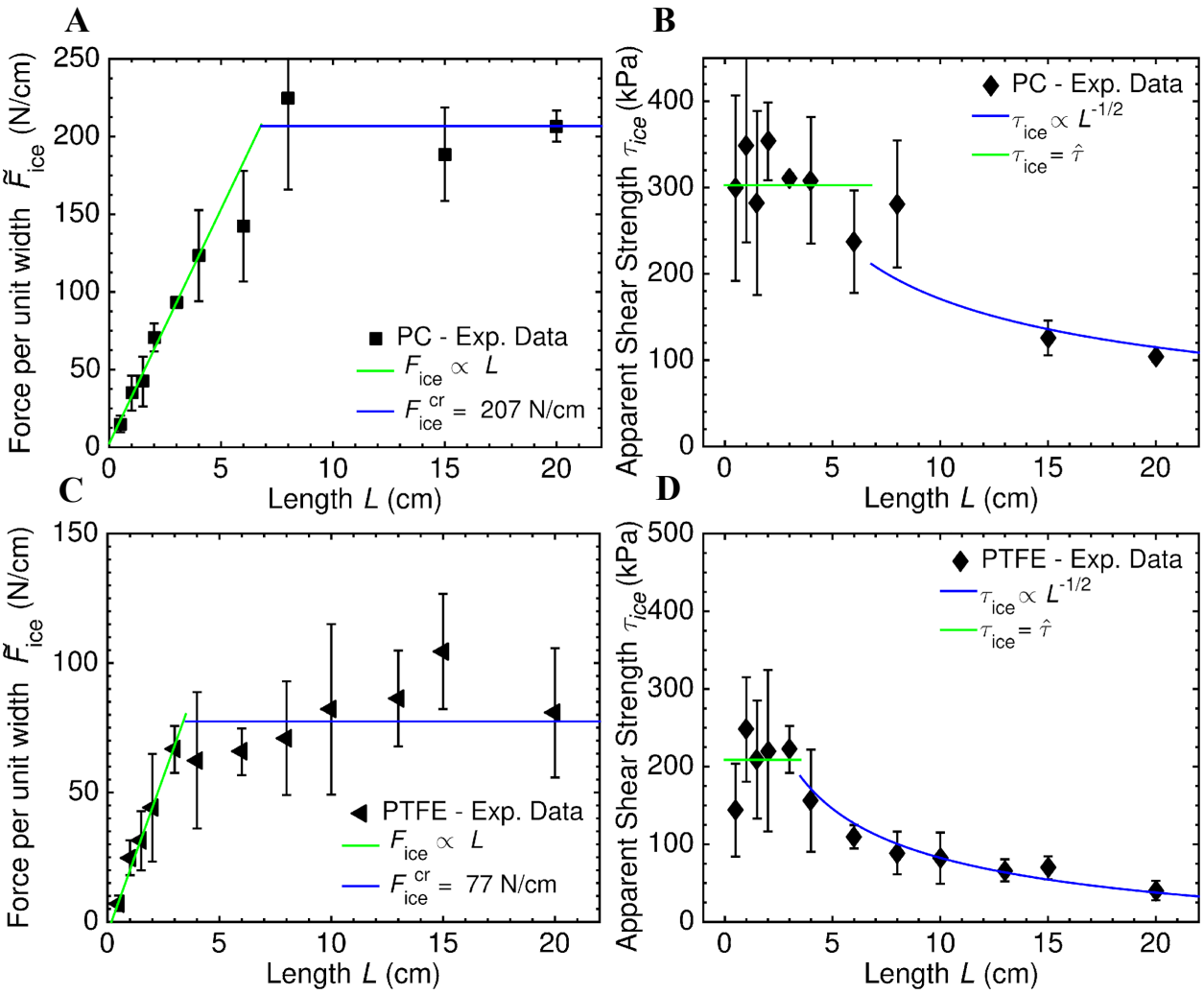

Figure S10. Fracture of ice from PC and PTFE. (A) The force per unit width required to detach adhered ice from PC. **(B)** The apparent ice-adhesion strength of PC (1.6 mm thick). After $L_c = 6.5$ cm, the force became constant and τ_{ice} began to decrease. At $L = 20$ cm, $\tau_{ice} = 103 \pm 11$ kPa. **(C)** The force per unit width required to detach ice from PTFE. **(D)** The apparent ice-adhesion strength of PTFE (1.6 mm thick). After $L_c = 3.5$ cm, the force became constant and τ_{ice} began to decrease. At $L = 20$ cm, $\tau_{ice} = 39 \pm 3.9$ kPa. Error bars denote 1 standard deviation ($N \geq 5$).

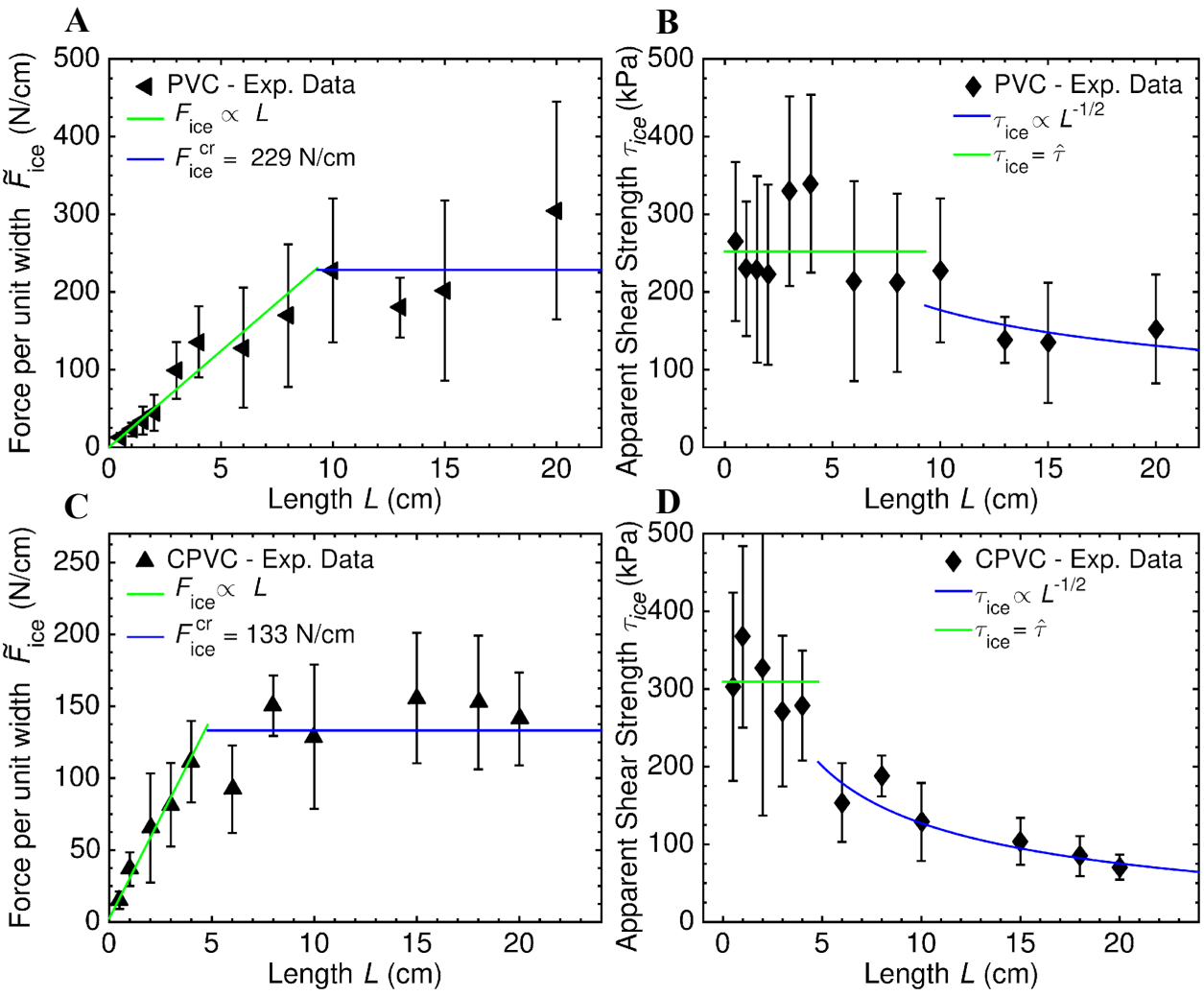

Figure S11. Fracture of ice from PVC and CPVC. (A) The force per unit width required to detach adhered ice from PVC. **(B)** The apparent ice-adhesion strength of PVC (1.6 mm thick). After $L_c = 9.3$ cm, the force became constant and τ_{ice} began to decrease. At $L = 20$ cm, $\tau_{ice} = 114 \pm 26$ kPa. **(C)** The force per unit width required to detach ice from CPVC (1.6 mm thick). **(D)** The apparent ice-adhesion strength of CPVC. After $L_c = 5.6$ cm, the force became constant and τ_{ice} began to decrease. At $L = 20$ cm, $\tau_{ice} = 67 \pm 7.1$ kPa. Error bars denote 1 standard deviation ($N \geq 5$).

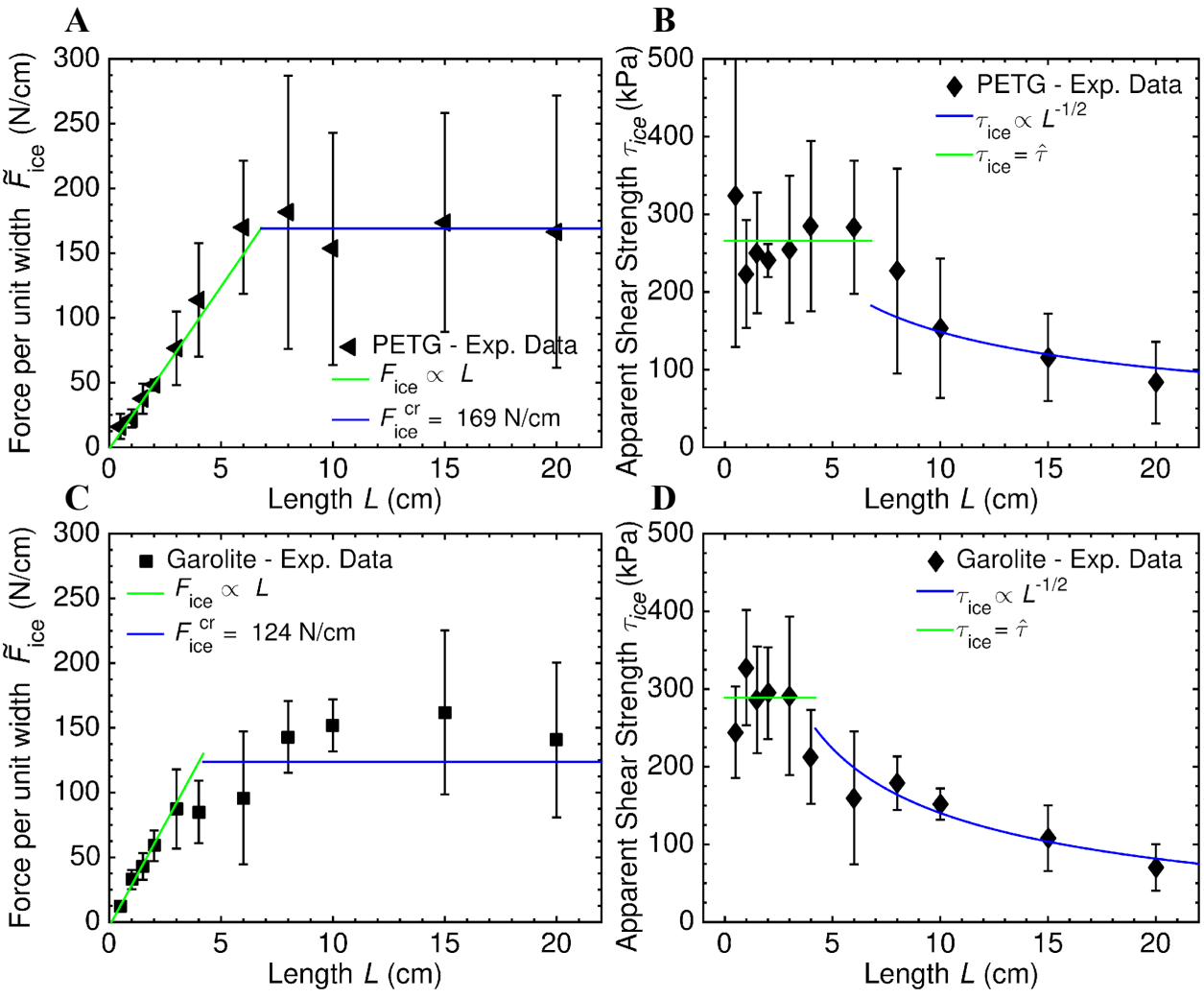

Figure S12. Fracture of ice from PETG and Garolite. (A) The force per unit width required to detach adhered ice from PETG. **(B)** The apparent ice-adhesion strength of PETG (1.6 mm thick). After $L_c = 6.8$ cm, the force became constant and τ_{ice} began to decrease. At $L = 20$ cm, $\tau_{ice} = 84 \pm 20$ kPa. **(C)** The force per unit width required to detach ice from Garolite. **(D)** The apparent ice-adhesion strength of Garolite (1.6 mm thick). After $L_c = 4.2$ cm, the force became constant and τ_{ice} began to decrease. At $L = 20$ cm, $\tau_{ice} = 70 \pm 29$ kPa. Error bars denote 1 standard deviation ($N \geq 5$).

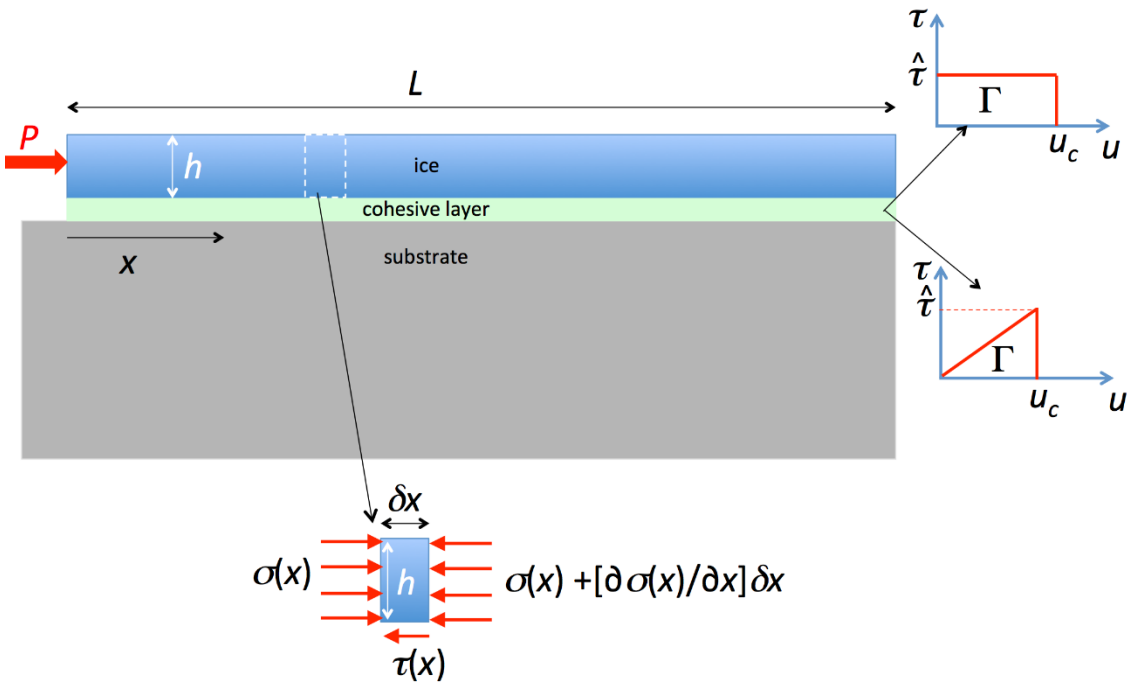

Figure S13. Schematic of a layer of ice of thickness *h* bonded over a length *L* to a thick substrate through a cohesive layer. One edge of the ice is loaded by a compressive force P (per unit width). The ice is assumed to have a modulus E, the substrate is assumed to be rigid, and only shear tractions from the cohesive layer are considered. Furthermore, the stresses in the ice are assumed to be uniform at each section.

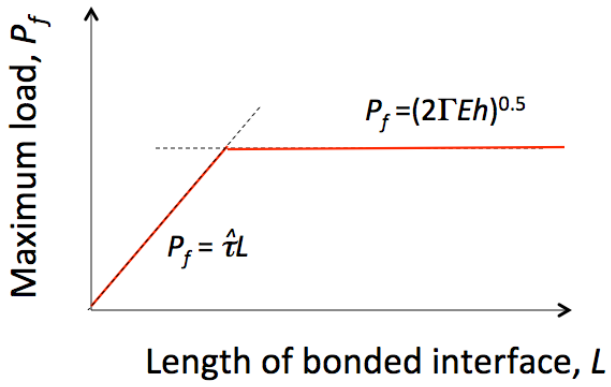

Figure S14. Variation of maximum load with the length of bonded interface. For the partial slip condition, $P_f = \sqrt{2\Gamma Eh}$ is the result for the toughness-limited regime. If there is full slip along the interface ($L = l_s$), then the requirement to maintain equilibrium dictates that the maximum load that can be applied is given by $P_f = \hat{\tau} L$. This is the strength-limited result.

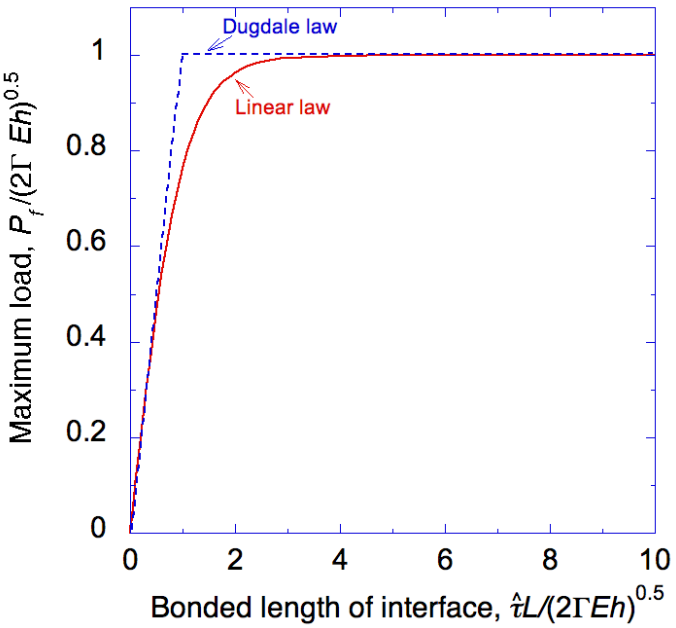

Figure S15. The load required to cause separation of the ice from the substrate. In this figure, the load is compared to that arising from the Dugdale (slip) analysis (as discussed in section 2E). For short and long bonded interfaces, the two distinct solutions from the Dugdale model (the strength and toughness regimes) emerge as asymptotes.

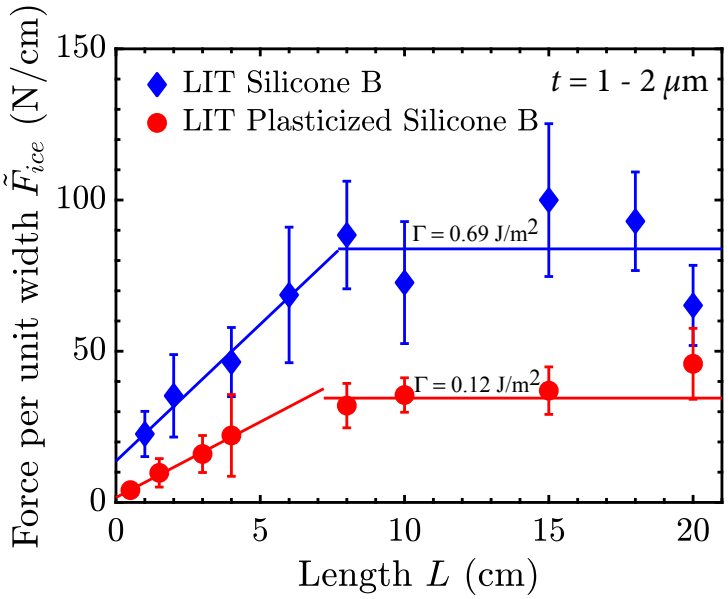

Figure S16. Slippage and toughness. The force necessary to remove ice adhered on two Silicone B surfaces, one plasticized and the other un-plasticized, both at -10 °C (Peltier). The plasticized silicone B has an ice adhesion strength of 115 kPa while the non-plasticized silicone B has an ice adhesion strength of 148 kPa. Only the plasticized Silicone B displays interfacial slippage. Error bars denote 1 standard deviation (N ≥ 5).

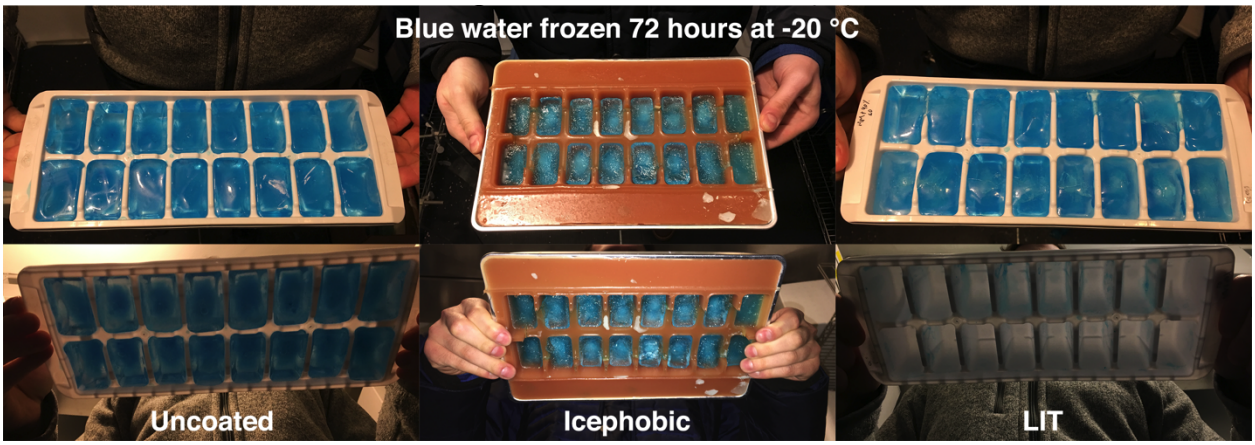

Figure S17. Ice-cube-tray experiment. Three ice-cube trays were filled with water (dyed blue for contrast) in a -20 °C freezer for 72 hours: an uncoated tray, a tray fabricated from an extremely icephobic material *(14)* (Section 1F), and a tray coated with our LIT PDMS (Table 1). Upon turning the trays upside-down, the ice remained adhered to both the uncoated and icephobic trays. Almost all ice cubes fell from the LIT tray when flipped, solely due to gravity, while the rest required minimal force to detach (Movie S4).

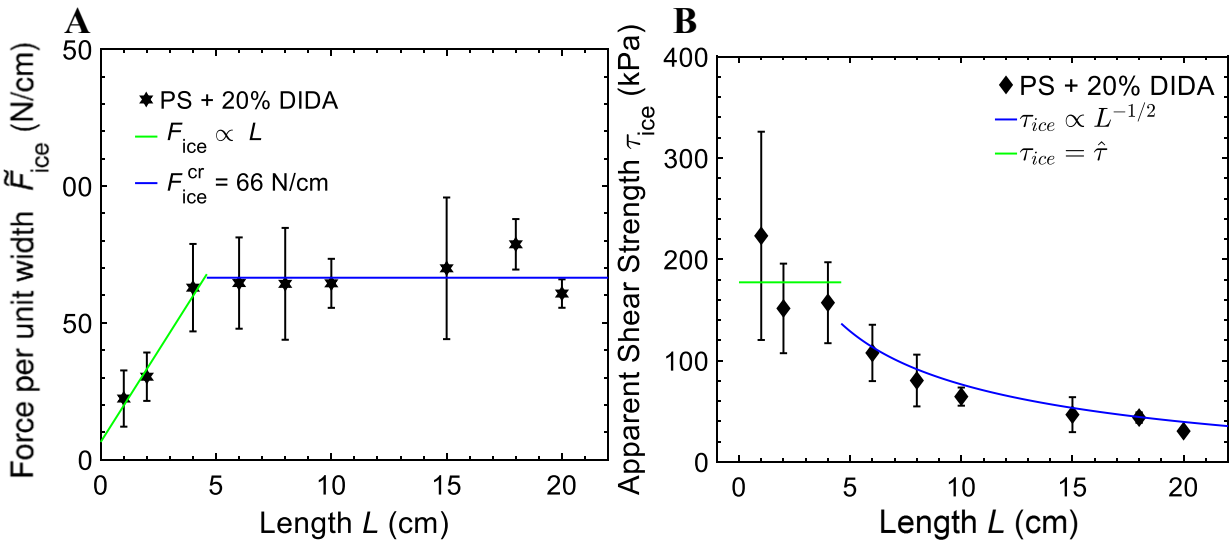

Figure S18. Fracture of ice from PS + 20wt% DIDA. (A) The force per unit width required to detach adhered ice from PS + 20wt% DIDA. **(B)** The apparent ice-adhesion strength of PS + 20% DIDA (1 μm thick). After $L_c = 4.6$ cm, the force became constant and τ_{ice} began to decrease. At $L = 20$ cm, $\tau_{ice} = 30 \pm 2.6$ kPa. Error bars denote 1 standard deviation ($N \geq 5$).

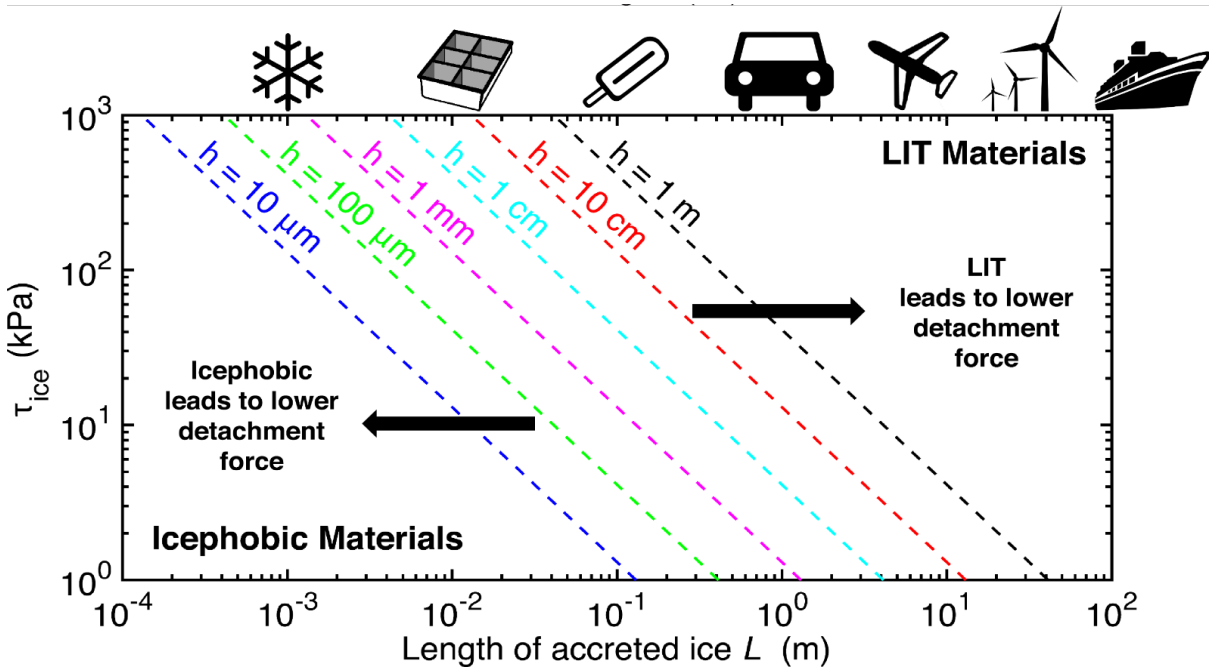

Figure S19. Significance of the length of accreted ice. The length of accreted ice determines if an icephobic material or a LIT material should be used for a given application. Based on the thickness (h) of accreted ice, there always exists a length beyond which a LIT material may be designed to exhibit a lower apparent ice-adhesion strength (τ_{ice}) than an icephobic material. A value of $\Gamma = 0.1$ J/m^2 is assumed for the LIT material in this plot. Note that decreasing the thickness of ice favors LIT materials, making them advantageous in situations where the ice needs to be removed before it grows to an appreciable size. The characteristic lengths of several relevant applications are also depicted in cartoon form. From left to right: a snowflake, an ice cube tray, a frozen confectionary, an automobile, an airplane, a wind turbine blade and a naval vessel.

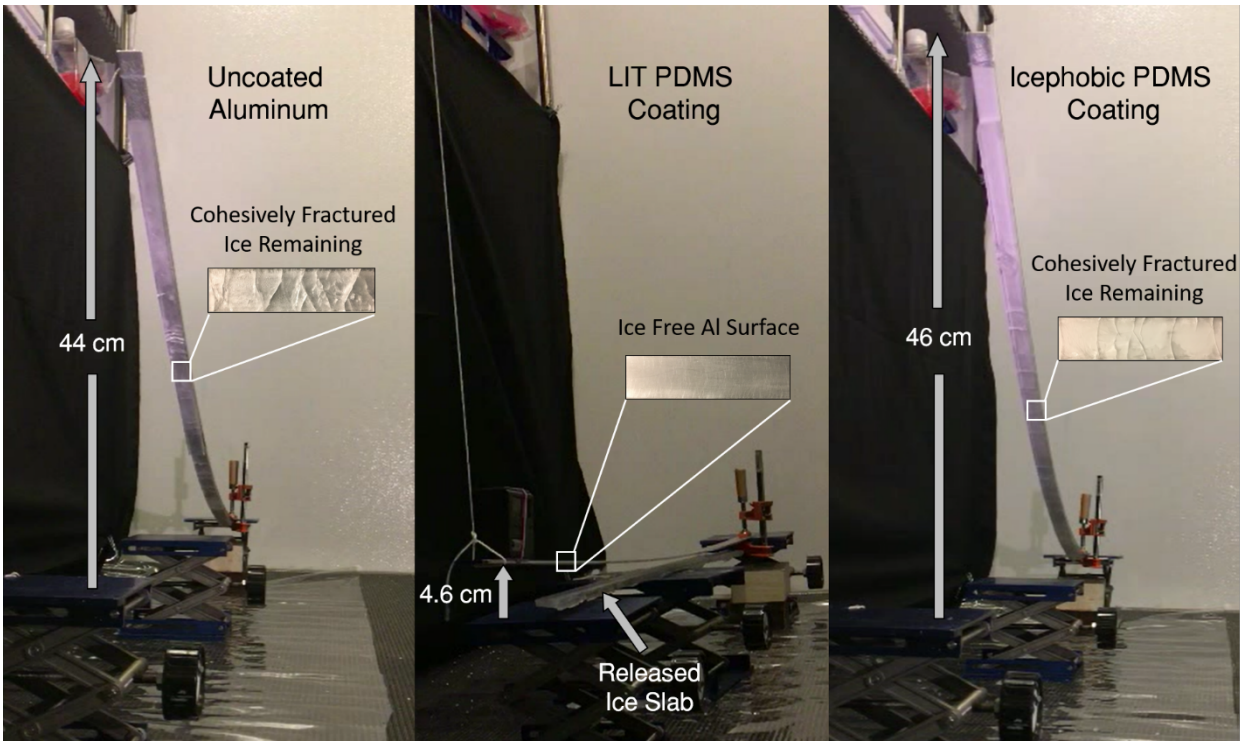

Figure S20. End-loaded cantilever beam tests. A comparison between uncoated and coated (with icephobic PDMS and LIT PDMS coating) aluminum beams adhered to a sheet of ice (1.0 m × 0.025 m × 0.008 m) undergoing end-loaded cantilever bending tests. The entire ice slab fractured cleanly from the beam coated with the LIT PDMS coating with an extremely low deflection of 4.6 cm. The uncoated and icephobic beams remained adhered to the ice sheet at severe deflections. The ice sheet displayed cohesive fracture from the uncoated and icephobic Al beams, as shown in the insets (Movie S3).

Supplementary Table

Surface	S_q (μm)
Silicone A	0.26 ± 0.10
Plasticized Silicone A	0.19 ± 0.15
Silicone B	0.71 ± 0.11
Plasticized Silicone B	0.59 ± 0.24
UHMWPE	3.30 ± 0.30
ABS	0.33 ± 0.03
PTFE	2.40 ± 0.10
CPVC	1.20 ± 0.20
LDPE	0.73 ± 0.02
PP	0.29 ± 0.13
PS	4.20 ± 0.10
PETG	0.15 ± 0.03
Garolite	2.06 ± 0.48
PMMA	0.16 ± 0.04
Nylon	0.35 ± 0.24
PC	0.10 ± 0.04
PVC	0.13 ± 0.02
LIT PS	0.44 ± 0.05
LIT PVC	0.40 ± 0.19
LIT PDMS	0.56 ± 0.11

Table S1. Root mean squared roughness (S_q) for the different surfaces considered in this work. The table above lists the different root mean squared roughness values for surfaces studied in this work. All the bulk plastics obtained from the distributor were unaltered before testing. Data uncertainty denotes 1 standard deviation ($N \geq 4$).

Captions for Movies S1-S5

Movie S1. Interfacial rupture vs. crack propagation with different lengths of ice. A comparison between the detachment of a 3 cm × 1 cm and 15 cm × 1 cm adhered ice block frozen over polyvinyl chloride (temperature = -10 ºC). Adhesion of the interface controls interfacial fracture for lengths of ice less than L_c (3.6 ± 0.7 cm for polypropylene), thus failure occurs through simultaneous rupture of the interface. Toughness of the interface controls fracture for the ice-polypropylene system for lengths of ice greater than L_c, thus fracture occurs via propagation of a crack.

Movie S2. Off-center-loaded cantilever beam tests. A comparison between uncoated, icephobic, and LIT aluminum beams adhered to a sheet of ice (1.0 m × 0.025 m × 0.008 m) undergoing off-center load flex tests. Ice fractured from the LIT-coated specimen with a remarkably low apparent ice adhesion strength of 0.39 kPa, while ice remained adhered to the uncoated aluminum and icephobic specimens even at severe deflections.

Movie S3. End-loaded cantilever beam tests. A comparison between uncoated and coated (with icephobic PDMS and LIT PDMS coating) aluminum beams adhered to a sheet of ice (1.0 m × 0.025 m × 0.008 m) undergoing end-loaded cantilever bending tests. The entire ice slab fractured cleanly from the beam coated with the LIT PDMS coating with an extremely low deflection of 4.6 cm. The uncoated and icephobic beams remained adhered to the ice sheet at severe deflections. The ice sheet displayed cohesive fracture from the uncoated and icephobic Al beams.

Movie S4. Ice-cube-tray flex test. A comparison between the performance of an uncoated and LIT PDMS coated PP ice-cube-tray frozen with water (dyed blue for contrast). Upon flipping the frozen trays upside-down, almost all the ice cubes fell from the LIT PDMS-coated tray, solely under the force of gravity. All the ice cubes remained well-adhered to the uncoated tray.

Movie S5. Large scale testing of LIT materials. An aluminum sheet coated with LIT PDMS before, during, and after fracture from a large sheet of ice (0.90 m × 0.90 m × 0.01 m). The weight of the ice sheet alone was sufficient to cause fracture, displaying an exceedingly low apparent ice adhesion strength of 0.09 kPa. A comparison is also made to uncoated aluminum.